X-ray fluorescence molecular imaging of high-Z tracers: investigation of a novel analyzer based setup

Bernhard H. Müller^{1,2}, Christoph Hoeschen², Florian Grüner³, Thorsten R. C. Johnson⁴

¹Ludwig Maximilian University of Munich, Department of Physics

²Helmholtz Zentrum München German Research Center for Environmental Health, Research Unit for Medical Radiation Physics and Diagnostics

³University of Hamburg, Department of Physics, Institute of Experimental Physics

⁴Ludwig Maximilian University of Munich, Department of Clinical Radiology

Abstract

A novel x-ray fluorescence imaging setup for the in vivo detection of high-Z tracer distributions is investigated for its application in molecular imaging. The setup uses an energy resolved detection method based on a Bragg reflecting analyzer array together with a multiple scatter reducing radial collimator. The aim of this work is to investigate the potential application of this imaging method to in vivo imaging in humans. A proof of principle experiment modeling a partial setup for the detection of gold nano-particles was conducted in order to test the feasibility of the proposed imaging method. Furthermore a Monte Carlo simulation of the complete setup was created in order to quantify the dependence of the image quality on the applied radiation dose and on the geometrical collimator parameters as well as on the analyzer crystal parameters. The Monte Carlo simulation quantifies the signal-to-noise ratio per radiation dose and its dependence on the collimator parameters. Thereby the parameters needed for a dose efficient in vivo imaging of gold nano-particle based tracer distributions are quantified. However also a number of problems are found like the fluorescence emission as well as scatter from the collimator material obscuring the tracer fluorescence and the potentially large scan time.

Keywords: x-ray fluorescence, molecular imaging, high-Z tracers, gold nanoparticles, Geant4 simulation

1 Introduction

X-ray computed tomography (CT) is one of the most important and widely applied diagnostic tools in clinical practice today. In addition to the contrast generated by anatomical structures, further diagnostic information can be obtained by using contrast agents containing high-Z elements like iodine, gadolinium or gold which have a high x-ray absorption coefficient. In order to detect these contrast agents spectral imaging techniques based on the characteristic energy dependence of the x-ray absorption coefficient have been developed for iodine in dual energy angiographic CT [1] and for gadolinium in energy resolving K-edge CT [2].

Conventional x-ray imaging, however, lacks functional information on the molecular level. Therefore there has been an increased interest in recent years in approaches towards molecular imaging with x-ray CT using gold nanoparticles conjugated to certain bio-molecules and it has been shown that specific tumor imaging can, at least in principle, be achieved [3, 4], although at tracer concentrations and radiation doses far too high for clinical imaging.

Absorption based imaging, however, is not the most dose efficient way of detecting very low concentrations of high-Z tracers and, as well known from material analysis and non-destructive testing, x-ray fluorescence imaging

Medical Imaging 2014: Physics of Medical Imaging, edited by Bruce R. Whiting, Christoph Hoeschen, Despina Kontos, Proc. of SPIE Vol. 9033, 90331J ⋅ © 2014 SPIE ⋅ CCC code: 1605-7422/14/\$18 ⋅ doi: 10.1117/12.2041948

can provide a much higher sensitivity. Simulation studies comparing x-ray fluorescence CT and K-edge absorption CT also indicate that fluorescence imaging can provide a better sensitivity for very low tracer concentrations [5].

While it has already been shown that in vivo x-ray fluorescence CT of iodine based tracers [6, 7, 8] and of gold nanoparticles [9, 5] appears conceivable using photon-counting energy resolving detectors, it has also been observed that there are a number of problems that prevent dose efficient imaging of lower tracer concentrations relevant for clinical molecular imaging [10]. Most importantly, the background signal resulting from Compton scattering leads to noise obscuring the fluorescence signal while the relatively large amount of Compton scattered x-rays may also incur dead time problems for photon-counting detectors. Secondly, a large detector area is needed in order to be dose efficient and sensitive as the fluorescence x-rays are emitted isotropically, which is problematic regarding the small area of the energy resolving detectors currently available. Furthermore, the energy resolution of the detector has to be good enough to distinguish the fluorescence signal in the spectrum from the Compton scattering background. At higher x-ray energies this is currently only provided by HPGe and CdTe detectors which are limited with respect to their sensitive area and their maximum count rate.

In order to solve these problems, we proposed a novel x-ray fluorescence imaging setup which uses a pencil beam generated from an x-ray tube with a high-kVp filtered spectrum together with a detection method based on the combination of a multiple scatter reducing radial collimator with an array of Bragg reflecting analyzer crystal leaves [8]. This detection method relys on the spectral separation of the tracer's K_{α} -fluorescence x-rays in an energy interval below the single scattered x-rays while filtering out non-radially directed multiple scattered x-rays using the radial collimator in combination with the energy selective Bragg reflection over a large detection area. We showed that for iodine based tracers, at least in principle, very low concentrations down to a few $\mu g/ml$ could be detected for in vivo imaging of iodine in small animals using this setup [8].

While a similar investigation [10] also suggested to use a higher energetic pencil beam in order to spectrally separate the tracer's K_{α} -fluorescence in an energy interval below the single scattered x-rays it did not attempt to filter out the remaining multiple scattered x-rays and did not use a large detection area resulting in a negative conclusion regarding the detection of low tracer concentrations.

The idea of using the reflection on an analyzer crystal in order to detect fluorescence x-rays has previously been proposed for use at synchrotron x-ray sources [11]. There a bent single crystal Laue analyzer has been used for detecting the lower energetic L-fluorescence of heavier elements as well as the K-fluorescence of lighter elements which, however, would be absorbed by the large amount of tissue in the case of human imaging.

While we previously showed that for iodine based tracers the proposed imaging method could be applicable to in vivo imaging of small animals [8] the aim of this work is to investigate the potential application of this imaging setup to in vivo imaging in humans. There, because of the attenuation of the x-rays by the body tissue, high-Z tracers having a higher energetic fluorescence emission like gold nanoparticles are more suitable. In order to test the the idea of using a Bragg reflecting crystal as energy selective filter we constructed a partial setup of the proposed imaging method in a proof of principle experiment for the detection of gold nanoparticles. Furthermore, we modeled the complete imaging setup with a Monte Carlo simulation using a simple human phantom containing gold nanoparticles. The Monte Carlo simulation is used to quantify the signal-to-noise ratio per radiation dose and its dependence on the collimator parameters and on the width of the analyzer crystal reflectivity curve. Thereby optimized parameters for a dose efficient in vivo imaging of gold nano-particle based tracers are found together with an estimation of the minimal detectable gold concentration.

2 Materials and Methods

2.1 Proposed x-ray fluorescence imaging setup

In the schematic diagrams of the proposed imaging setup, shown in figure 1, it can be seen that a pencil-beam created from the filtered and collimated output of an x-ray tube is used to scan an object containing a distribution of a high-Z tracer material. Using a high peak kilo-voltage for the x-ray tube results in a mean x-ray energy of its output well above the K-edge of the high-Z tracer, while the lower part of the output spectrum is filtered by a combination of absorber layers consisting of copper, tin or other suitable elements.

As the pencil beam passes through an object containing a distribution of a high-Z tracer like gold, the interaction of the x-rays with the tracer's atoms leads to the ejection of K-shell electrons which are then replaced

by outer shell electrons, followed by the radiation of characteristic x-rays. These fluorescence x-rays together with scattered x-rays due to the Compton effect then pass the radial collimator setup and are Bragg reflected by an array of crystal leaves onto a detector (c.f. side-view schematic diagram in figure 1). The detector itself would preferably be a large area scintillation detector providing a moderate energy resolution. As the angle of the crystal leaves is set to the Bragg angle corresponding to the energy of the K_{α} -fluorescence of the high-Z tracer, only x-rays near that energy are reflected by the first reflection order. Supporting the crystal by an absorbing layer ensures that the transmitted x-rays do not reach the detector. As the lower part of the pencil beam spectrum is filtered out, apart from the fluorescence x-rays, only multiple scattered x-rays are contained in this reflected energy region as the energy loss in one instance of Compton scattering is limited. The radial collimator in turn leads to a partial rejection of these multiple Compton scattered x-rays, as a large amount of them is directed non-radially.

Thus, the energy specific Bragg reflection of the fluorescence on the crystal leaves together with the highenergy incident spectrum and the rejection of the majority of multiple scattered x-rays by the collimator results in a selective detection of the tracer's x-ray fluorescence. The fluorescence yield depends on the concentration and the length of tracer distribution on the course of the pencil beam within the object. The filtering of a large part of the scattered x-rays by the radial collimator and the energy selective reflection on the crystal leaves also ensure that count-rate limitations of the detector are not violated even in large objects and at high x-ray fluxes.

Planar images of the spatial distribution of a high-Z tracer material are then created by scanning the pencil beam over the object along two dimensions as indicated by the x- and y-axis in figure 1 while recording the detected x-rays together with the corresponding scan position.

The analyzer crystal leaves should have a high reflectivity over an angular range corresponding to the pencil beam cross section diameter. This is for example provided by mosaic crystals like highly oriented pyrolytic graphite (HOPG) which is an artificially produced crystal structure. In particular HOPG has a mosaic structure consisting of crystallites with a certain width of their angular distribution called mosaic spread which is typically around 0.4°. This gives HOPG the largest integrated reflectivity of all known crystals of up to 30% in the energy interval between 50 and 70 keV. Although the relatively large mosaic spread comes at the expense of a moderate energy resolution when compared to single crystals it has the advantage that the cross section diameter of the pencil beam can be in the range of 1 mm.

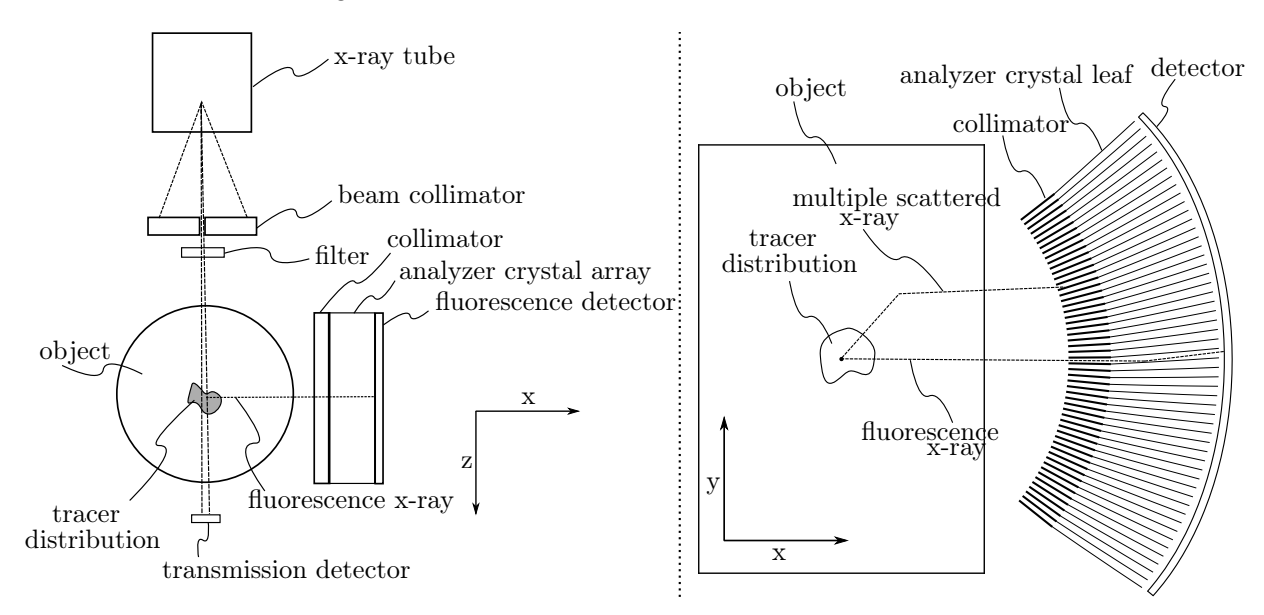


Figure 1: Left: Top view schematics of the proposed x-ray fluorescence imaging setup. Right: Side view schematics of the proposed x-ray fluorescence imaging setup.

2.2 Monte Carlo simulation of the proposed x-ray fluorescence imaging setup

The proposed imaging setup and the dependence of its imaging performance on the parameters of the setup can be accurately modelled using general purpose Monte Carlo simulations of the interaction of x-rays with matter. In this work the Geant4 Monte Carlo toolkit [12] has been used to create a simulation of the proposed imaging setup implementing the geometry and all relevant beam characteristics. The physics processes implemented in this simulation provide an accurate model of the passage of x-rays through the imaged phantom in particular of the absorption, fluorescence and scattering processes.

The phantom used in the simulation is modelled as a water cylinder with a diameter of 20 cm. In the center of this body cylinder there is a smaller inner cylinder with a diameter of 1 cm which contains a mixture of gold and water. A schematic diagram of the phantom geometry is shown in figure 2.

The sensitive area of the detector is modelled by an enclosing tube along the axis defined by the pencil beam direction with a length of 50 cm and a diameter of 50 cm. The detector is placed at an offset of 0.25 m in the forward z-direction as this detection range in the longitudinal direction corresponds to a small scattering angle of the single scattered x-rays which are not scattered down to a much lower energy. Therefore the incident energy can be lowered when detecting only at those smaller angles resulting in a larger fluorescence cross-section. Ideally it would be better to detect also in the backwards direction and to use an angular weighting factor. The energy resolved detection of the x-rays has been implemented as an ideal detector with a predefined energy bin size.

Two different models of the collimator have been implemented. The first one consists of an idealized angular filter with an angular acceptance threshold corresponding to the angular width defined by the collimator leaf spacing and length. This simplified model of the collimator rejects all x-rays deviating from the radial direction by an angle greater than a predefined angular acceptance threshold. The second collimator model consists of a more realistic implementation of the collimator leaves which takes into account the interaction of the scattered and fluorescence x-rays with the collimator material. We have chosen molybdenum as collimator material in the simulation as its fluorescence is spectrally separated far enough from the gold fluorescence. This is not the case for lead or tungsten as the energy of their K-fluorescence emissions are close to that of gold. Tin has also been considered as collimator material but it did not show a better performance in the simulation when compared to molybdenum.

The first image formation step in the simulation is represented by scanning the pencil beam together with the detector and collimator over the object, in the x-y plane as shown in figure 1, while recording for each scan position the contribution of the x-rays hitting the detector to each energy bin. This effectively gives a spectrum at each scan position from which an image of the tracer distribution is then created by a multiplication of this spectrum with the reflectivity curve of the crystal under the Bragg angle corresponding to the K_{α} -fluorescence energy of gold at approximately 68 keV. The crystal reflectivity curve has been implemented here using a normal distribution with a standard deviation corresponding to the width of the reflectivity curve. Throughout this work, an idealized peak reflectivity of 1 has been assumed and the scan resolution is set to a value of 2 mm.

However, there is still a significant amount of Compton scattered x-rays in the energy bins around the tracer's fluorescence energy, which results in a relevant amount of background noise. The attenuation of the pencil-beam and of the scattered x-rays depends on the scan position because of the variable thickness of the finite phantom volume resulting in a spatial variation of this background noise level. Therefore, an attenuation correction has to be done. This is best done by using the information from the attenuation of the pencil-beam as shown in [13, 14]. As this has not yet been implemented in our simulation, we applied a least-squares fit using a fourth degree polynomial to the background, which should be sufficient in this case because of the relatively simple phantom geometry.

Using this simulation model we investigated the optimization of several parameters of the proposed imaging method. At first we quantified the dependence of the minimal detectable gold concentration on the incident pencil beam energy using an idealized collimator model. Secondly by simulating the imaging procedure using the more realistic collimator model we quantified the dependence of the minimal detectable gold concentration on the collimator leaf spacing. In both of these investigations the minimal detectable gold concentration is defined as the concentration needed for attaining a signal-to-noise ratio (SNR) of 5 at a mean absorbed dose of 10 mGy. The minimal detectable concentration was calculated from the results of the simulations, which were done at a higher value of the gold concentration and a lower dose, by extrapolating to the concentration needed

for attaining a SNR of 5 at a dose of 10 mGy. The SNR was calculated according to SNR = $S_{K_{\alpha}}/\sqrt{\sigma_{K_{\alpha}}^2 + \sigma_b^2}$ for a detected number of K_{α} -fluorescence x-rays given by $S_{K_{\alpha}}$ and for a variance of the detected fluorescence and of the background scattering signal given by $\sigma_{K_{\alpha}}^2$ and σ_b^2 respectively while the extrapolation is based on assuming poisson statistics.

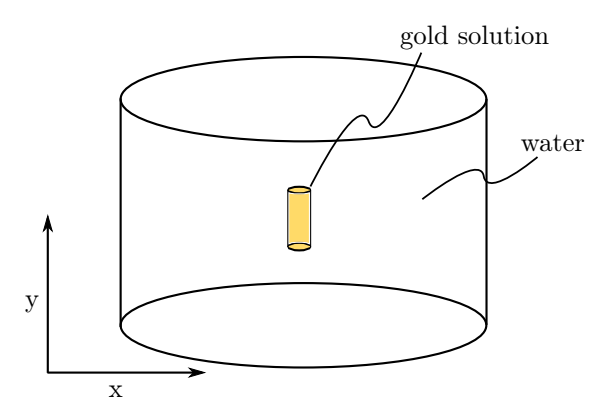


Figure 2: Geometry of the phantom for the Monte Carlo simulation of in vivo imaging.

2.3 Proof of principle experiment

In order to test the idea of using a Bragg-reflecting analyzer crystal as energy filter for selectively detecting the K_{α} -fluorescence of the tracer we constructed an experimental setup using a single layer of a HOPG mosaic crystal with a mosaic spread of 0.4°. As shown in the schematic diagram in figure 3, a pencil beam hits a sample containing a gold solution resulting in the emission of x-ray fluorescence which is reflected by the HOPG layer at an angle of approximately 1.54° onto an energy resolving photon-counting detector (XR-100T-CdTe, Amptek Inc.). The sample used in this measurement consists of a tube with a diameter of 1 cm filled with a gold solution at a concentration of 1 mg/ml. The pencil beam is created by a lead hole collimator with a diameter of 1.5 mm which is placed at the exit window of an x-ray tube with a tungsten anode operating at a peak kilo-voltage of 200 kVp together with a 4 mm thick Aluminum filter and a 5 mm thick copper filter. The distance between the pencil beam and center of the crystal is approximately 12 cm. A collimator slit at the point of reflection and a lead hole collimator in front of the detector ensure that only reflected x-rays should be detected. In contrast to the proposed complete imaging setup which relys on the energy selection of the Bragg reflection in combination with a simple large area detector, the CdTe detector used in this experiment provides a high energy resolution which gives detailed information about the reflected x-ray spectrum, which can be used to diagnose and optimize the properties of the setup.

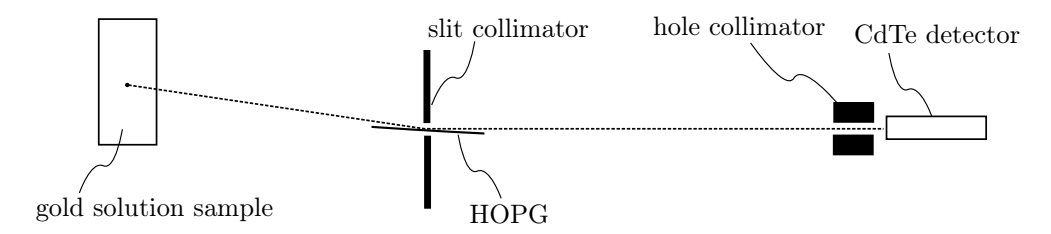


Figure 3: Schematics of the experimental setup.

3 Results

3.1 Simulation with idealized collimator model

Simulation of the imaging method using the human phantom (cf. figure 2) was performed as described above by scanning the pencil-beam in the x-y plane while recording the detected x-ray spectrum multiplied by the analyzer reflectivity curve at every scan step. For an idealized set of parameters the resulting attenuation corrected image for a gold concentration of 100 µg/ml is shown in figure 4 together with a plot of the spectrum corresponding to the detector signal averaged over the scanned volume of the gold solution cylinder. This simulation was done using the idealized collimator model with an angular acceptance threshold of 0.01° which filters out a significant amount of multiple scattered x-rays. Therefore the image shown in figure 4 clearly shows the location of the gold cylinder even at an absorbed dose of only 0.73 mGy for a monochromatic 100 keV pencil beam and for an assumed width of the reflectivity curve of 1 keV.

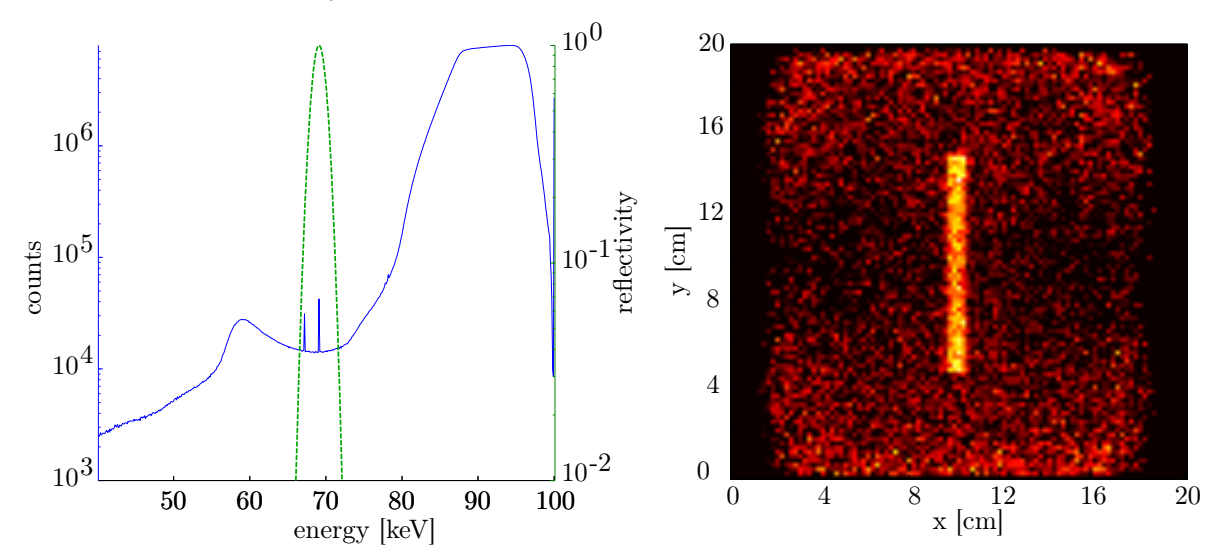


Figure 4: Left: Logarithmic plot of the detected x-ray spectrum averaged over the scanned volume of the 100 µg/ml gold solution cylinder of the human phantom for an energy bin size of 100 eV. The normal distribution (dashed, green) corresponds to the reflectivity curve of the analyzer crystal. The standard deviation of the energy-reflectivity curve is 1 keV.

Right: Attenuation corrected fluorescence image showing the position of the 100 µg/ml gold solution cylinder. The corresponding scanning pencil beam is mono-energetic at 100 keV and is scanned at a step size of 2 mm. The mean absorbed dose deposited in the human phantom is 0.73 mGy. The angular acceptance threshold of the collimator is 0.01° .

As it is unclear if these parameters can be practically achieved we simulated the imaging procedure for a more realistic angular acceptance threshold of the collimator of 0.1° in order to quantify the minimal detectable gold concentration. The imaging simulation was done for different values of the pencil beam energy and for different values of the width of the crystal reflectivity curve and the minimal gold concentration was estimated by extrapolating to the concentration needed for attaining an SNR of at least 5 at a mean absorbed dose of 10 mGy. As shown in figure 5 the minimal detectable gold concentration increases for larger values of the width of the reflectivity curve where more noise from multiple scattered x-rays is detected. The dependence of the minimal detectable gold concentration on the pencil beam energy shows that the optimal pencil-beam energy for the most sensitive detection is in the range of 90 keV to 110 keV. This results from the fact that there is a trade-off between the increased noise from detecting single scattered x-rays at lower pencil beam energies and the decreasing fluorescence cross section at higher pencil beam energies. It can also be observed that the optimal pencil beam energy depends on the width of the crystal reflectivity curve which can only be countered by using a higher pencil beam energy.

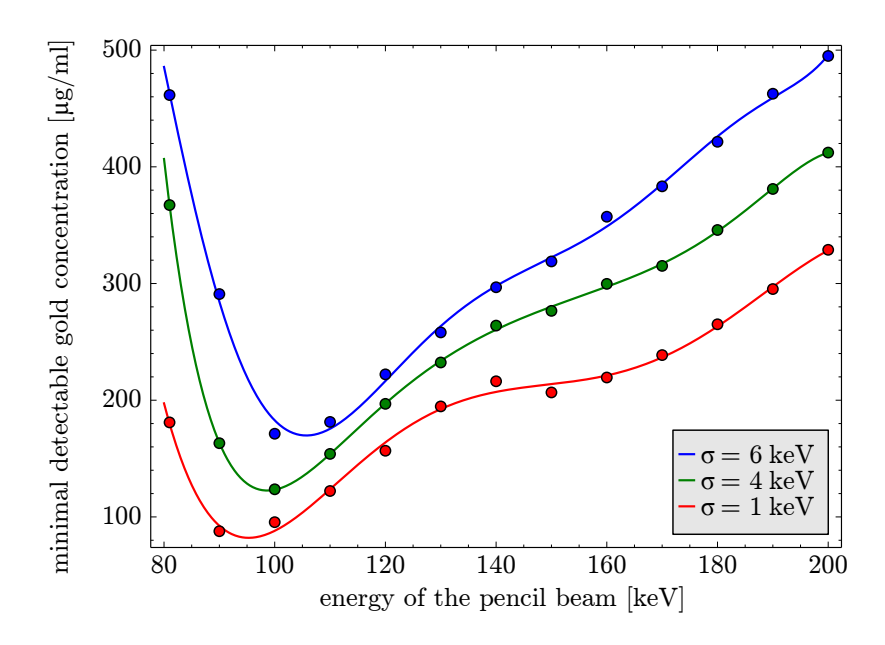


Figure 5: Gold concentration needed for attaining a SNR of 5 at a mean absorbed dose of 10 mGy plotted against the pencil beam energy for different widths of the crystal reflectivity curve σ .

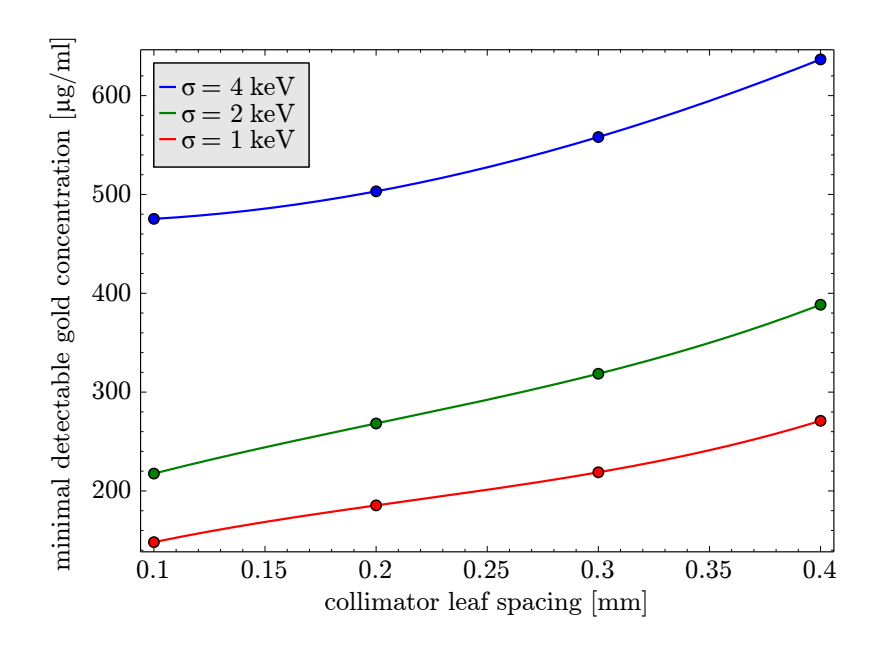


Figure 6: Gold concentration needed for attaining a SNR of 5 at a mean absorbed dose of 10 mGy plotted against the collimator leaf spacing for different widths of the crystal reflectivity curve σ .

3.2 Simulation with realistic collimator model

The idealized collimator model did not account for absorption due to the finite width of the collimator leafs and it also negelects the effects of transmission and scattering occurring in the collimator material. Therefore we simulated the imaging procedure using an implementation of the collimator geometry in Geant4 accounting for the interaction of the scattered x-rays with the collimator material. We have chosen the element molybdenum for the collimator material as other heavier elements, which have good absorption properties, like tungsten and lead emit fluorescence x-rays at an energy close to the fluorescence energy of gold. The simulation was done for a pencil beam energy of 100 keV, a collimator leaf thickness of 0.02 mm and a leaf length of 50 mm. In figure 6, which shows a plot of the minimal detectable gold concentration depending on the collimator leaf spacing, it can be seen that the performance of the realistic collimator is significantly worse than in the idealized case leading to an increased minimal detectable concentration. This could result from the incomplete absorption of the scattered x-rays by the thin collimator leaves and from the fact that a very small collimator leaf spacing is needed in order to effective filter out most of the multiple scattered x-rays. The finite thickness of the collimator leafs, however, should only account for a reduction of the fluorescence signal of less than 20%.

3.3 Proof of principle experiment

A simple experiment was constructed as described above, measuring the reflection of the gold fluorescence on a single layer of HOPG (cf. figure 3). The spectrum of the x-rays recorded by the energy resolving detector is shown in figure 7.

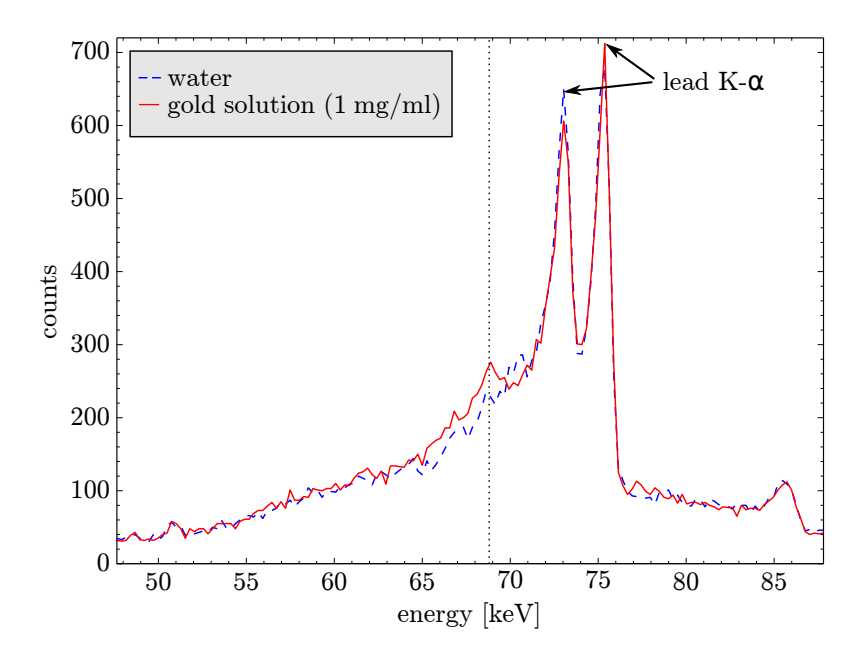


Figure 7: Spectrum of the x-rays reflected by a single layer of HOPG in the proof of principle experiment for a water sample and for a gold solution sample with a gold concentration of 1 mg/ml. The location of the gold K_{α_1} fluorescence is indicated by the dotted line.

This allows us to test the idea of using Bragg reflection on a crystal layer as energy filter and shows the difficulties involved in this detection method. Although the K_{α_1} fluorescence emission of gold is visible in the spectrum, the first problem, which is to be expected, results from the fluorescence emission of the lead collimators. As the lead fluorescence is separated from the gold fluorescence by only 4 keV this obscures the much smaller signal of the tracer fluorescence. This could, however, be overcome by using collimators and shieldings made of lighter elements like molybdenum or tin, as shown in the simulation.

The second and main problem results from the large width of the reflectivity curve of about 10 keV which is a consequence of the crystal mosaicity of 0.4°. This would make it difficult to use only the crystal reflection for selecting an energy interval around the gold fluorescence and would lead to the detection of a large amount of scattered x-rays. Using a crystal with a smaller mosaic spread or a bent single crystal could, however, solve this issue.

Furthermore the small Bragg angle of 1.54° results in the reflection of x-rays from only a very small solid angle for a single crystal layer which necessitates the use of multiple reflecting layers for detecting over a larger solid angle.

4 Discussion and Outlook

An x-ray fluorescence imaging setup has been investigated for its application to in vivo molecular imaging in humans. The detection method used in this setup is based on the spectral separation of the K_{α} -fluorescence x-rays of gold nanoparticle based tracers in an energy interval below the single scattered x-rays while filtering out non-radially directed multiple scattered x-rays using a radial collimator combined with the energy selective Bragg reflection on a crystal.

Although this approach requires a scanning pencil-beam for providing spatial resolution it appears to be more sensitive when compared to fan beam approaches [9, 15]. By simulating the image generation with an idealized collimator model and assuming a width of the crystal reflectivity curve of 1 keV we have shown that by using a monochromatic 100 keV pencil beam a tracer concentration of 100 µg/ml can be detected. This sensitivity is mainly achieved by filtering out the multiple scattered x-rays and by using a large detection area. A more detailed simulation, however, taking into account the transmission and scattering of x-rays in the collimator material shows that a small collimator leaf spacing in the range of about 0.1 mm to 0.4 mm would be required and that the incomplete absorption and the scattering in the collimator material leads to an increase of the minimal detectable tracer concentration by a factor of 2 to 4 depending on the parameters of the collimator and of the crystal.

A proof of principle experiment has been conducted using a single layer of HOPG in order to test the efficiency of the analyzer based energy selection. It has been shown that the large mosaic spread of the crystal leads to a low energy resolution which would prevent the efficient detection of a low tracer concentration. This could be overcome by using a different crystal structure with a smaller mosaic spread or by using a bent single crystal.

The use of a pencil beam also potentially results in a large scan time because most of the flux of the x-ray source is blocked by the beam-collimator and a first generation CT technique has to be applied in order to generate slice images. As also noted in [10] this appears to be one of the main problems which could prevent a practical application to in vivo imaging. We estimate the scan time corresponding to the simulated projection images shown in this work to be in the range of several minutes when using the heavily filtered output of a clinically used x-ray tube which would result in an acquisition time far too high for in vivo imaging especially when generating CT images.

However, it may be possible to construct pencil beam x-ray sources which have a higher flux than currently available sources used in clinical x-ray imaging by using alternative x-ray tube constructions [16]. Also novel laser-driven quasi-monoenergetic x-ray sources based on undulator radiation [17, 18] are perfectly suited to the proposed imaging setup because of their pencil beam output free from lower energetic x-rays.

If the mentioned obstacles can be overcome then the proposed method would open up the opportunity of using x-ray fluorescence imaging for detecting tracers based on gold nanoparticles conjugated to bio-molecules which appears to be a promising approach towards specific tumor imaging.

Acknowledgements

This work has been financially supported by the DFG Cluster-of-Excellence 'Munich-Centre for Advanced Photonics' MAP.

References

- [1] Johnson, T. R., Krauss, B., Sedlmair, M., Grasruck, M., Bruder, H., Morhard, D., Fink, C., Weckbach, S., Lenhard, M., Schmidt, B., Flohr, T., Reiser, M. F., and Becker, C. R., "Material differentiation by dual energy CT: initial experience," *European Radiology* 17(6), 1510–1517 (2007).
- [2] Schlomka, J. P., Roessl, E., Dorscheid, R., Dill, S., Martens, G., Istel, T., Bäumer, C., Herrmann, C., Steadman, R., Zeitler, G., Livne, A., and Proksa, R., "Experimental feasibility of multi-energy photon-counting K-edge imaging in pre-clinical computed tomography," *Physics in Medicine and Biology* 53(15), 4031 (2008).
- [3] Popovtzer, R., Agrawal, A., Kotov, N. A., Popovtzer, A., Balter, J., Carey, T. E., and Kopelman, R., "Targeted Gold Nanoparticles Enable Molecular CT Imaging of Cancer," Nano Letters 8(12), 4593–4596 (2008).
- [4] Hainfeld, J. F., O'connor, M. J., Dilmanian, F. A., Slatkin, D. N., Adams, D. J., and Smilowitz, H. M., "Micro-CT enables microlocalisation and quantification of Her2-targeted gold nanoparticles within tumour regions.," *The British journal of radiology* (2010 Nov 16 2010).
- [5] Bazalova, M., Kuang, Y., Pratx, G., and Xing, L., "Investigation of X-ray Fluorescence Computed Tomography (XFCT) and K-Edge Imaging," *Medical Imaging, IEEE Transactions on* **31**(8), 1620–1627 (2012).
- [6] Cesareo, R. and Mascarenhas, S., "A new tomographic device based on the detection of fluorescent x-rays," Nuclear Instruments and Methods in Physics Research Section A: Accelerators, Spectrometers, Detectors and Associated Equipment 277(2–3), 669 672 (1989).
- [7] Takeda, T., Wu, J., Thet-Thet-Lwin, Huo, Q., Yuasa, T., Hyodo, K., Dilmanian, F. A., and Akatsuka, T., "X-ray fluorescent CT imaging of cerebral uptake of stable-iodine perfusion agent iodoamphetamine analog IMP in mice," *Journal of Synchrotron Radiation* 16, 57–62 (Jan 2009).
- [8] Müller, B. H., Hoeschen, C., Grüner, F., Arkadiev, V. A., and Johnson, T. R. C., "Molecular imaging based on x-ray fluorescent high-Z tracers," *Physics in Medicine and Biology* **58**(22), 8063 (2013).
- [9] Jones, B. L., Manohar, N., Reynoso, F., Karellas, A., and Cho, S. H., "Experimental demonstration of benchtop x-ray fluorescence computed tomography (XFCT) of gold nanoparticle-loaded objects using leadand tin-filtered polychromatic cone-beams," *Physics in Medicine and Biology* **57**(23), N457 (2012).
- [10] von Busch, H., Harding, G., Martens, G., Schlomka, J.-P., and Schweizer, B., "Investigation of externally activated x-ray fluorescence tomography for use in medical diagnostics," *Proc. SPIE, Medical Imaging* 2005: *Physics of Medical Imaging* 5745(90), 90–101 (2005).
- [11] Karanfil, C., Zhong, Z., Chapman, L. D., Fischetti, R., Bunker, G. B., Segre, C. U., and Bunker, B. A., "A bent Laue analyzer detection system for dilute fluorescence XAFS," *AIP Conference Proceedings* **521**(1) (2000).
- [12] Agostinelli, S. et al., "Geant4: a simulation toolkit," Nuclear Instruments and Methods in Physics Research A 506, 250–303 (2003).
- [13] Hogan, J., Gonsalves, R., and Krieger, A., "Fluorescent computer tomography: a model for correction of x-ray absorption," *Nuclear Science*, *IEEE Transactions on* **38**(6), 1721–1727 (1991).
- [14] Bazalova, M., Ahmad, M., Pratx, G., and Xing, L., "L-shell x-ray fluorescence computed tomography (XFCT) imaging of Cisplatin," *Physics in Medicine and Biology* **59**(1), 219 (2014).
- [15] Jones, B. L. and Cho, S. H., "The feasibility of polychromatic cone-beam x-ray fluorescence computed to-mography (XFCT) imaging of gold nanoparticle-loaded objects: a Monte Carlo study," *Physics in Medicine and Biology* **56**(12), 3719 (2011).

- [16] Cao, G., Lu, J., and Zhou, O., "X-ray fluorescence molecular imaging with high sensitivity: feasibility study in phantoms," *Proc. SPIE, Medical Imaging 2012: Physics of Medical Imaging* **8313**(6) (2012).
- [17] Fuchs, M., Weingartner, R., Popp, A., Major, Z., Becker, S., Osterhoff, J., Cortrie, I., Zeitler, B., Hörlein, R., Tsakiris, G. D., Schramm, U., Rowlands-Rees, T. P., Hooker, S. M., Habs, D., Krausz, F., Karsch, S., and Grüner, F., "Laser-driven soft-x-ray undulator source," *Nature Physics* 5 (2009).
- [18] Müller, B. H., Schlattl, H., Grüner, F., and Hoeschen, C., "A laser-driven undulator x-ray source: simulation of image formation and dose deposition in mammography," *Proc. SPIE, Medical Imaging 2011: Physics of Medical Imaging* **7961**(6) (2011).

Proc. of SPIE Vol. 9033 90331J-11